Theoretical description of alkali metal *closo*-boranes – towards the crystal structure of $MgB_{12}H_{12}$

Aristea E. Maniadaki,* and Zbigniew Łodziana,‡

Solid state *closo*-borane salts of alkali metals have very high ionic conductivity. This makes them interesting for practical applications as a solid state electrolytes, and triggers extensive research efforts. Improvement and understanding of their properties require accurate theoretical description of static and dynamical properties. In this work, we report accuracy assessment of Density Functional Theory in description of solids with $B_{12}H_{12}{}^{2-}$ anions. We show that these aromatic anions are interacting via weak dispersive forces. For that reason, non-local exchange - correlation functionals give better description of structural properties and phonons in $Li_2B_{12}H_{12}$ and $Na_2B_{12}H_{12}$. Numerically efficient semi-local methods provide satisfactory results when applied in structure volumes obtained in non-local method. Extensive structural search for stable crystalline phases of $MgB_{12}H_{12}$ predicts new denser lattice with $C2/c$ symmetry that is stabilized by Van der Waals interactions. These structures might be discovered as anhydrous $MgB_{12}H_{12}$ in the high pressure experiments, avoiding amorphous state at ambient pressures.

1 Introduction

An almost four decades old idea of using *closo*-boranes in solution as an electrolyte in rechargeable batteries[1] is booming recently due to the discovery of superionic conductivity in solid state sodium *closo*-dodecaborate[2]. This material has sodium conductivity competing with a standard β-alumina, thus it could serve as a solid state ionic conductor targeting to rechargeable batteries with high power density, high stability, and ultimate safety. The replacement of the present organic electrolytes with solid state ones could be a key to developing such solid state batteries[3]. Several new discoveries of superionic conductivity in polyborane salts[4–8], that followed the first report[2], established new class of solid state electrolytes with ionic conductivity exceeding 0.01 S/cm at 297 K[6].

Variety of new inorganic superionic compounds were reported recently (with lithium conductivity of the order 0.01 S/cm at room temperature, that is rivaling with liquid electrolytes); these materials are usually based on oxides[9] or sulfides;[10] they consists of four or more distinct elements, and their crystal structure is rather complex. The crystal lattice is formed by three dimensional framework skeleton with metal-oxygen or metal-sulfur coordination polyhedra (MO_4 or MO_6) and channels for facile cation diffusion. Complex chemistry of these materials often correlates with poor electrochemical stability. On the contrary ionic conductors based on *closo*-boranes are structurally very simple compounds, with somehow complex anions arranged on body centered cubic (*bcc*) or cubic close packed (*ccp*) sublattice. The superionic state is accompanied with anion orientational disorder and configurational disorder of cations. Transition to the superionic state can be related to the structural transition with change of anion packing, like *ccp* - *bcc* ($P2_1/c \rightarrow Pm\bar{3}n \rightarrow Im\bar{3}m$) transition in $Na_2B_{12}H_{12}$[11] or it can be related to the lattice expansion within the same anion arrangement, like $Pa\bar{3}$ and $Fm\bar{3}m$ phases of $Li_2B_{12}H_{12}$.[11] At low temperatures these materials possess well defined ordered crystal structure.

The polyhedral *closo*-boranes anions represent a class of compounds with three center two electron bonds[12]. Closed deltahedral structures with formula $B_nH_n{}^{2-}$ have $2n+2$ skeletal electrons, with number of vertices $6 \leq n \leq 12$. Addition of skeletal electrons leads to more open *nido* or *arachno* structures according to Wade rules.[13] Replacement of boron with carbon atom in one or two vertices leads to monoanions like monocabra-*closo*-boranes ($CB_{n-1}H_n{}^-$) or neutral carboranes like dicabra-*closo*-boranes ($C_2B_{n-2}H_n$). Compounds with anions like: $B_{12}H_{12}{}^{2-}$, $B_{10}H_{10}{}^{2-}$, $CB_{11}H_{12}{}^-$, $CB_9H_{10}{}^-$ and their combinations constitute solid state superionic conductors with the highest conductivity in the class[4–7]. The $B_{12}H_{12}{}^{2-}$ anion is a regular icosahedron while $B_{10}H_{10}{}^{2-}$ is a bicapped square antiprism. Both have triangular faces; there are 5 edges meeting at each vertex except 4 edges meeting at two capping vertices of $B_{10}H_{10}{}^{2-}$. They are also the

Institute of Nuclear Physics, Polish Academy of Sciences, ul. Radzikowskiego 152, PL31-342 Kraków, Poland. Fax: +48 12 6628458; Tel: +48 12 6628267; E-mail: * aristea.maniadaki@ifj.edu.pl, ‡ zbigniew.lodziana@ifj.edu.pl

† Electronic Supplementary Information (ESI) available: [details of any supplementary information available should be included here]. See DOI: 10.1039/b000000x/

most stable anions in the range of vertices $6 < n \leq 12$.

Already in the 70-ties Aihara pointed out three-dimensional aromatic nature of polyhedral boranes[14]. This observation is based on unusual thermal and chemical stability of anions mentioned above; in analogy with the stability of two-dimensional polygonal molecules like benzene. In addition, these polyhedral boranes $B_nH_n^{2-}$ with $n = 10, 12$ exhibit delocalized bonding, with some bonding electrons fully delocalized within the cage structure.[15]

Understanding of superionic properties of solid state *closo*-borane compounds is aided by theoretical calculations mostly based on Density Functional Theory (DFT). Already some aspects related to anion/cation combinations and correlations;[16] anion reorientation and cation hoping[17]; electrochemical stability;[18] disorder[19] or structure[20] were investigated. DFT methods are used to describe the low temperature structure as well as the dynamical properties and atomic motion in the high temperature polymorphs via *ab initio* molecular dynamics or transition state theory. Due to large lattice expansion/changes the proper description of the high temperature phases require further attention due to potential deficiency of extrapolation from the low to high temperature structures. One of the problems is related to the description of the interatomic forces by local exchange-correlation functionals routinely used in DFT. Non-local weak dispersive forces originate from intrinsic charge fluctuations and they require special treatment in DFT. Charge fluctuations of delocalized electrons in aromatic systems like *closo*-anions cannot be neglected. In the simplest way it can be described as pairwise additive Van der Waals interactions ($\sim C_6/r^6$) that originate from the second order perturbation theory. They can be implemented without any significant computational cost in DFT codes. Thus this approach is the most widespread and successfully used within DFT calculations[21,22]. Methods that go beyond pairwise interactions are available[23]. Their importance is growing recently, especially when used for molecular or aromatic systems[24,25]. In fact, van der Waals attraction between C60 molecules is responsible for the formation of fullerene crystalline structure[26].

Below we report detailed analysis of the structural, electronic and vibrational properties of lithium, sodium and magnesium *closo*-dodecaborates. The analysis of the charge distribution indicates they are strongly ionic systems. Non-covalent interaction analysis indicates weak dispersive interaction between $B_{12}H_{12}^{2-}$ anions and cations. We show that the most accurate description of these compounds is provided by non-local method, and pairwise Van der Waals corrections strongly underestimate the lattice parameters for $Li_2B_{12}H_{12}$ and $Na_2B_{12}H_{12}$. Pairwise approximations applied for the correct volume of these compounds provides satisfactory phonon spectra. Based on this analysis of two known compounds we report on the crystal structure of $MgB_{12}H_{12}$. New crystal phases of this compound are proposed. They have higher density than any structure of this compound reported till now. This suggest that solvent free anhydrous $MgB_{12}H_{12}$ can be possibly characterized experimentally under high pressure.

2 Computational Details

The calculations are performed within density functional theory (DFT) as implemented in the Vienna *Ab initio* Simulation package (VASP)[27–30]. Technical details are presented in the ESI†. Independent calculations accounting for a weak dispersion interactions were performed for GGA exchange correlation functional. We have considered parameterized approach by Grimme: PBE-D2[21] and PBE-D3 with with Becke-Jonson(BJ) damping[22];van der Waals density functional (vdW-DF)[23,31–33]; as well as hybrid functionals PBE0[34] and HSE06[35]. Further technical details related to phonon calculations, charge density analysis and thermodynamic stability are presented in ESI†.

3 Results

In the following sections calculations of the properties of known low temperature structures of $Li_2B_{12}H_{12}$ and $Na_2B_{12}H_{12}$ are discussed in the framework of approximations to the exchange - correlation functional. The structural, electronic, dynamical as well as thermodynamic properties are presented with the conclusion that proper description of dispersive forces is important for solids with closo-borane molecules. Based on these results the low temperature crystal structure of $MgB_{12}H_{12}$ is revisited and new denser structure with $C2/c$ symmetry is proposed along with additional possible structures with P*nna*, $P4_2m$ and $P2_1$ space groups.

3.1 $Li_2B_{12}H_{12}$ and $Na_2B_{12}H_{12}$

Closo - boranes were subject to intensive studies over the past decades[12,13,36–39]. Recently, the discovery of high ionic conductivity in alkali metal dodeca- or deca- boranes renewed interest in these materials as potential solid state electrolytes[40,41]. Together with detailed experimental characterization[11,42–44] theoretical models of ion conductivity are published[16–20]. Here we focus on two representative compounds: $Li_2B_{12}H_{12}$ and $Na_2B_{12}H_{12}$.

3.1.1 Ground state properties

At low temperatures $Li_2B_{12}H_{12}$ crystallizes in $Pa\bar{3}$ symmetry where anions are arranged in *ccp* configuration[42,43]. Around $T = 615$ K[11] this structure undergoes phase transition to the $Fm\bar{3}m$ symmetry. Anions remain in *ccp* arrangement, but they are orientationally disordered; cations occupy fraction of the available interstitial sites with trigonal coordination to anions. The $Na_2B_{12}H_{12}$ adopts $P2_1/c$ crystal structure at low temperatures[11]. This compound undergoes transition to the disordered cubic $Pm\bar{3}n$ phase at 513 K and $Im\bar{3}m$ phase at 563 K[44]. At elevated temperatures alternatively the $Fm\bar{3}m$ at $T = 519$ K structure is observed[20]. The low temperature structures of $Li_2B_{12}H_{12}$ and $Na_2B_{12}H_{12}$ are shown in Fig. 1. The cations of each compound are coordinated to three anions. Each of the high temperature phases shows a high ionic conductivity.

Theoretical *ab initio* description of superionic properties of these structures requires insight into rare events related to cation hoping and to disorder - both occurring only at high temperatures. Thus, methods like molecular dynamics or nudged elastic band have to be applied. In principle, this well established ap-

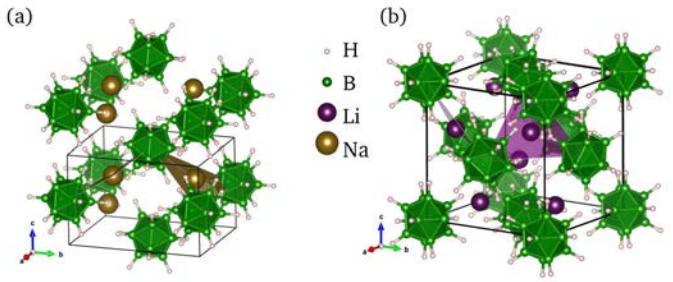

Fig. 1 The unit cells of the low temperature phase of (a) $Na_2B_{12}H_{12}$ and (b) $Li_2B_{12}H_{12}$. For $Na_2B_{12}H_{12}$ the neighboring in the z direction cell is also shown, for a more clear view of the ions packing. The green polyhedra indicate the B_{12} icosahedra. The purple triangular planes indicate the coordination of Li and the brown triangular planes the coordination of Na.

proach shall be straightforward for simple electronic structures as in the case of *closo*-borane salts of alkali metals. However, for even simpler anion BH_4^- a standard local formulation of DFT is insufficient. The importance of long-range dispersive interactions in a proper description of the ground state of $Mg(BH_4)_2$ was pointed out before [45,46]. For this compound only use of non-local van der Waals density functional (vdW-DF) leads to a good agreement with experimental crystal structure [45]. In the *closo*-borane salts the aromatic nature of the deltahedral molecules ($B_{12}H_{12}^{2-}$, $B_{10}H_{10}^{2-}$) is an additional factor calling for consideration of the weak dispersion forces. The *closo*-borane molecules form quasi-spherical objects as such having a strong long-range van der Waals attraction. The weak adhesive interaction between spherical particles is a classical effect with the interaction energy proportional to $1/r$, r separation between particles. [47] In the microscopic level dispersive interaction between aromatic molecules is well known [24]. Such situation calls for the critical accuracy assessment of *ab initio* approach for salts with $B_{12}H_{12}^{2-}$ or similar anions. The description of the ground state properties together with harmonic excitation shall provide a measure of the accuracy.

We have considered different approaches of the density functional theory to calculate the ground state of $Li_2B_{12}H_{12}$ and $Na_2B_{12}H_{12}$: local density approximation (LDA) [48], generalized gradient approximation (PBE-GGA) [49], semi-empirical dispersion corrections implemented as the PBE-D2 [21], PBE-D3(BJ) [22], non-local method vdW-DF [23,31–33] as well as hybrid functionals PBE0 [34] and HSE06 [35]. For these molecular systems there are two important descriptors of the structure: the lattice parameters of the crystalline phase and the local structure of anions. The ground state structures are visualized in Fig. 1 and structural properties are presented in the Table ST2 (ESI†). When compared to the experimental low temperature crystallographic data, a usual performance of DFT is observed: LDA underestimating lattice parameters and GGA slightly overestimating. The semi-empirical method PBE-D2 underestimates the lattice parameters, while non-local electron gas method and hybrid functionals provide very good agreement with experimental data.

We compare the volume per formula unit in Fig. 2(a). The semi-empirical methods significantly underestimate the volume while vdW-DF method, PBE and hybrid functionals provide excellent accuracy with respect to volume per formula unit. The structure of alkali metal *closo*-boranes consists of electrostatically interacting metal cations and poly-anions. Due to the attractive Van der Waals interaction within semi-empirical methods interatomic attraction is overestimated since metal - hydrogen interaction is overestimated. Semi-empirical methods refer to the pairwise interaction between all atoms and consequently they strongly underestimate the lattice parameters. However, examination of the $B_{12}H_{12}^{2-}$ anion reveals that both semi-empirical methods provide consistent description of the icosahedral structure that is very close to the experimental values, see Fig. 2(b).

The experimental dimensions of the $B_{12}H_{12}^{2-}$ icosahedra are rather scattered when collected for several structures as shown in Fig. 2(b)(yelow points). This is related to difficulties in the determination of the boron positions for orientationally disordered molecules. Among all experimental data the low temperature neutron scattering for $Na_2B_{12}H_{12}$ seems to be the most accurate (green horizontal line in Fig.2(b)); to the best of our knowledge such data are not available for $Li_2B_{12}H_{12}$. When comparing the volume of B_{12} cage in $P2_1/c$ structure of $Na_2B_{12}H_{12}$ one can notice that this volume is significantly underestimated within the LDA approximation; the PBE provides excellent agreement that is also observed for semi-empirical methods. On the contrary, the volume of the icosahedra is larger when calculated with vdW-DF method and smaller with hybrid functionals. Van der Waals interactions could be repulsive on triangular lattices, like faces of icosahedra. Interestingly, all methods provide consistently similar volume of the B_{12} cage for Na- and Li- based compounds. The spread of boron - boron distances corresponds to the distortion of the icosahedra. This distortion is largest for semi-empirical methods, and smallest for local exchange correlation functionals. The large distortion for the semi-empirical methods originates from overestimated Van der Waals interaction between cations and terminal hydrogen atoms. This can be also observed for larger distortion for $Na_2B_{12}H_{12}$ when dispersive interaction is taken into account. Both hybrid functionals give the same range of distortion of the icosahedra, slightly underestimating its range. It is important to note that distortion of B_{12} icosahedra is not equivalent to the distortion of entire anion; where B - H bond length and angle can vary, depending on the environment. We have performed additional calculations where semi-empirical method PBE-D2 was applied for the system with the lattice parameters constrained to the geometry calculated with vdW-DF method (denoted as PBE-D2*). In Fig. 2(b) it is clear that such procedure provides good description of anion structure.

The interatomic distances related to the position of ions in the unit cell are shown in Fig. S4(a,b) (ESI†). The GGA, both vdW-DF method, PBE-D2* and also hybrid functionals, give very good agreement with the experimental data, while semi-empirical methods as well as LDA underestimate atomic separation. Since the semi-empirical method is much less demanding the present result indicates that use of parameterized Van der Waals potentials are justified for structural description when the lattice parameters are constrained to values calculated with more accurate vdW-DF method.

Strongly ionic nature of both compounds is confirmed by Bader

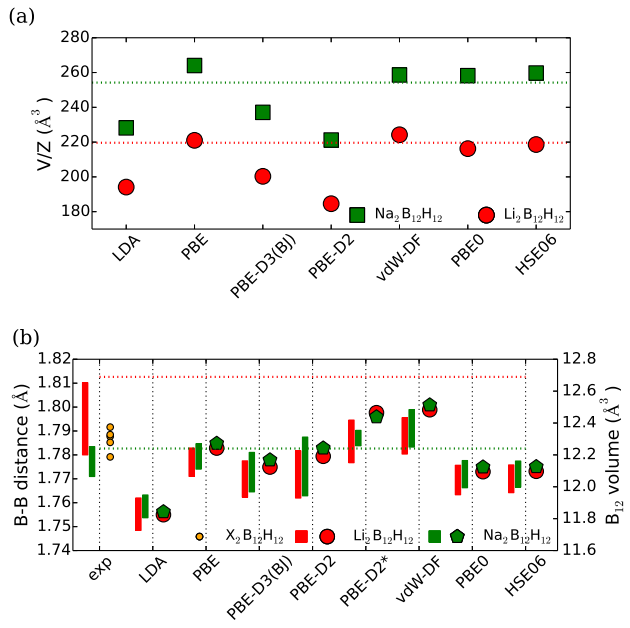

Fig. 2 (a) The volume per formula unit of the ground state structures of $Na_2B_{12}H_{12}$ (green squares) and $Li_2B_{12}H_{12}$ (red circles) calculated with different approximations of the exchange correlation functional. (b) the volume of the B_{12} icosahedral cage together with the range of the nearest B-B distances (vertical bars). The experimental volume and B_{12} cage volume for $Na_2B_{12}H_{12}$ are based on Ref. [11] and for $Li_2B_{12}H_{12}$ on Ref. [42] and are denoted with horizontal dashed green and red lines respectively. The yellow circles refer to B_{12} cage volume reported for other *closo*-dodecaboranes [50,51]

charge analysis, Table ST2 (ESI†). The calculated charge of $B_{12}H_{12}$ anion is -1.85 e for $Na_2B_{12}H_{12}$, and -1.90 e for $Li_2B_{12}H_{12}$. Both compounds are insulators with band gap larger than 5.1 eV, see Fig. S5 (ESI†). The analysis presented above provides a consistent picture of the two structures, however there is no clear indication for the superiority of one approach. In order to get more insight into the nature of the interactions in the *closo*-boranes considered here we perform more detailed charge density analysis.

3.1.2 Non Covalent Interaction Analysis

The topological analysis of the charge density could provide the real space visualization of the bonding within the crystal or molecular structures. The methods that rely on the analysis of the electron density gradients, like electron localization function (ELF) provide information about covalent bonds [52], while the information on weak dispersive interaction require more sophisticated approach. This can be achieved through the so called Non Covalent Interaction (NCI) analysis. This method is designed to visualize the charge density ρ in the regions where $\rho \simeq 0$. The analysis is based on the reduced density gradient $s = \frac{1}{2(3\pi^2)^{1/3}} \cdot \frac{|\nabla\rho|}{\rho^{4/3}}$ where ρ is the charge density. Additionally the eigenvalues of the Laplacian ($\Delta\rho$) are analyzed such, that the value of the second eigenvalue (λ_2) distinguishes the type of an interaction [53]. The bonding interactions are present for $\lambda_2 < 0$ and non-bonding interactions are for $\lambda_2 > 0$. The region where both the reduced density gradient $s \simeq 0$ and $\lambda_2 \simeq 0$ corresponds to the weak dispersive interactions.

The NCI analysis for $Li_2B_{12}H_{12}$ is presented in Fig.3. The reduced density gradient s, for all the interactions within the unit cell is shown in green color in Fig.3(a). Within the software it is possible to isolate two fragments of the unit cell and investigate their interaction. The interaction only between two neighbouring $B_{12}H_{12}{}^{2-}$ anions is shown in black, and the interaction only between an anion and the cations of the unit cell in red. It is clear that the covalent interactions within anions dominate the NCI plot (negative values of the horizontal axis). The dispersive interaction between anions is also pronounced for $\rho \simeq 0$. The

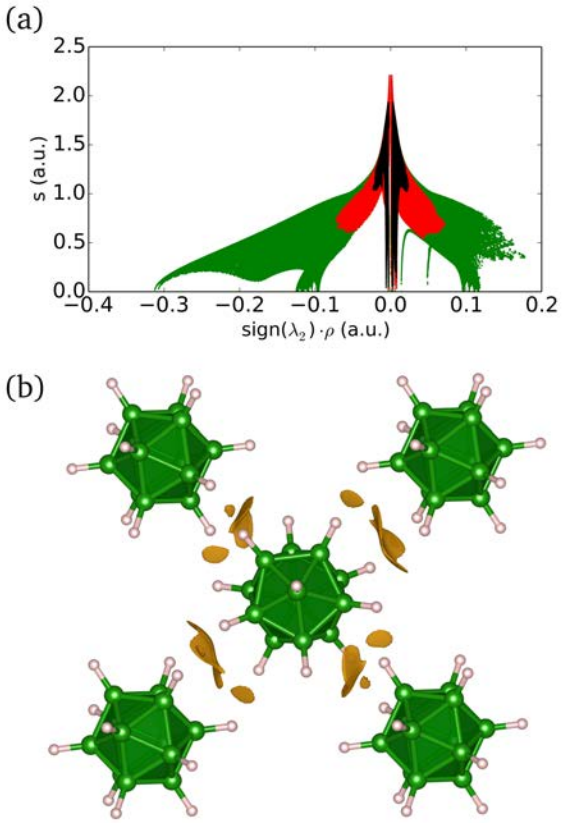

Fig. 3 (a)Reduced density gradient (s) plot for $Li_2B_{12}H_{12}$. Green, black and red denote the interactions between all components of the unit cell, between two neighbouring $B_{12}H_{12}$ anions and between the cations and one of the anions respectively. (b) Visualization of the isosurface indicating the noncovalent weak interactions between two neighbouring $B_{12}H_{12}$ anions. For better visualization only the two neighbouring $B_{12}H_{12}$ anions with also the additional periodic atoms are shown. The isosurface corresponds to s=0.5 a.u. and -0.01<ρ<0.01 a.u.

isosurface of the reduced charge density related to anion - anion interaction is visualized in Fig.3(b): the location of the reduced charge density gradients between anions represent Van der Waals interaction between them. The corresponding graphs of these interaction for $Na_2B_{12}H_{12}$ are presented in Fig. S6 (ESI†).

The charge density analysis clearly points out the presence of weak non-covalent interactions in alkali metal *closo* boranes. The origin and the consequences of these interactions for the properties of the systems will be discussed below.

3.1.3 Vibrational properties

The interaction between constituent elements in compounds has a principal role on the structure, however the dynamical properties such as atomic vibrations critically depend on type of interatomic forces and the structure symmetry. Calculation of the phonon spectra, in the harmonic approximation, is a simple way to access lattice dynamics. Harmonic approximation is also relevant for calculations of perfectors within transition state theory when applied to ion diffusion. Thus, the phonon density of states is a good probe for accuracy of structure description within DFT.

For complex molecular structures like the *closo*-borane salts considered here, the phonon spectrum consists of separated regions: the low frequency part represents lattice modes, this part of the spectrum is sensitive to cation-anion interaction and the crystalline lattice symmetry. The middle part of spectrum is related to internal vibrations of $B_{12}H_{12}^{2-}$ anion thus vibration frequencies calculated for this region depend on the accuracy of bonding forces within anion as well as interaction with cations distorting the icosahedral symmetry. The highest frequency part of the spectrum is related to stretching vibration of B-H bonds, which is sensitive to the distortion of an anion and the accuracy of covalent B-H bond description.

The phonon density of states (pDOS) were calculated with a finite difference method; atomic displacements of 0.02 Å were used. Three approximations for the exchange-correlation functional were used for these calculations: PBE, PBE-D2, and vdW-DF. Additional set of calculations was performed for the structures with the lattice parameters from vdW-DF and the dispersion interaction described within PBE-D2, it is denoted as PBE-D2*. For the accuracy assessment phonon density of states of $Na_2B_{12}H_{12}$ calculated with linear response method and high plane wave cutoff are presented in Fig. S7 (ESI†). The minor differences originate from the numerical errors. This assures validity of the present real space approach. The phonon density of states are presented

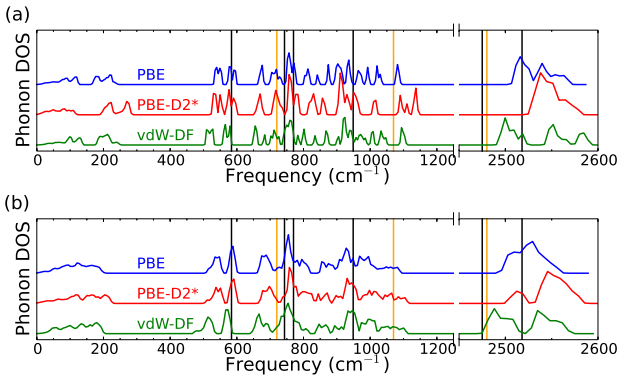

Fig. 4 Phonon density of states for $Li_2B_{12}H_{12}$(a) and for $Na_2B_{12}H_{12}$(b). For both structures the spectra shown are calculated with different methods, PBE, PBE-D2* and vdW-DF denoted with blue, red and green respectively. Additionally, the experimental peaks measured by Muetterties *et al.* [38] are shown with black (Raman) and orange (IR) lines.

in Fig.4. For $Li_2B_{12}H_{12}$ the lattice modes calculated with PBE and vdW-DF methods extend to 250 cm^{-1}, while for PBE-D2* method the low frequency part extends to 300 cm^{-1}. In the sodium counterpart the lattice modes cover the range up to 200 cm^{-1} due to larger mass of Na ($m_{Li}/m_{Na} \approx 0.3$). For this compound PBE-D2* lattice modes extend to 220 cm^{-1}. The internal $B_{12}H_{12}^{2-}$ modes cover the frequency range from 500 cm^{-1} to 1150 cm^{-1}. Since, they originate from the icosahedral anion the structure of this part of the spectrum should be similar for both compounds. Experimental results by Mutterties *et al.* [38] indicate that the T_{1u} infrared active modes related to internal vibration of $B_{12}H_{12}^{2-}$ appear at 720 cm^{-1} and 1070 cm^{-1} , the Raman active H_g modes are located at 584 cm^{-1}, 770 cm^{-1} and 949 cm^{-1}. The Raman A_g is at 743 cm^{-1}. In the crystalline salts these Raman modes are shifted [54,55] and their positions are marked with vertical lines in Fig. 4. The phonon density of states measured by neutron inelastic scattering for $Na_2B_{12}H_{12}$ [44] and $Li_2B_{12}H_{12}$ [42], provide internal $B_{12}H_{12}^{2-}$ modes at *ca.* 548 cm^{-1}, 580 cm^{-1}, 678 cm^{-1}, 766 cm^{-1}, 952cm^{-1}, 1008cm^{-1}. This complex vibration structure can be seen for calculated phonon spectra for $Na_2B_{12}H_{12}$: low frequency modes (H_u and H_g [56]) around 530 cm^{-1} and 580 cm^{-1} are best reproduced with vdW-DF method, other methods overestimate them by ∼30 cm^{-1}. The G_g around 678 cm^{-1} mode not observed by optical methods is again well reproduced by vdW-DF method with similar overestimation by the two other methods. Modes related to G_u, A_g, T_{2u} and H_g are grouped around 770 cm^{-1} again best reproduced with vdW-DF method. Peaks located around 950 cm^{-1} related to G_g, H_u , H_g and T_{1g} modes are underestimated with PBE method, while both methods accounting for Van der Waals forces locate them at a proper position. The highest frequency internal T_{1u} modes are again underestimated with local functional. Similar pattern can be observed for $Li_2B_{12}H_{12}$, see Fig. 4, however the phonon spectra for this compound is more complex due to larger distortion of anion icosahedra. High frequency internal modes are overestimated with PBE-D2* method for this compound. Both methods accounting for dispersion forces provide slightly broader spectrum than the local one, especially at lower frequencies where breathing modes of the anion are present.

In the stretching region of B-H bonds the calculated frequencies are overestimated, that is a known deficiency of DFT methods [57]. The accuracy for the absolute values of stretching frequencies are in the range of 2%. The vdW-DF method provides good description of the stretching vibrations splitting due to distortion of the anions and direct interaction of the cation with hydrogen. Particularly, for $Na_2B_{12}H_{12}$, the measured Raman modes H_g and Ag_g appear at 2494cm^{-1} and 2521cm^{-1} (marked as solid vertical lines in Fig. 4) are seen as double peak with vdW-DF method. For $Li_2B_{12}H_{12}$ stretching modes are located at 2475cm^{-1} and 2543cm^{-1} [54,55], further splitting of higher frequency modes is observed in the calculated spectrum.

3.1.4 Thermodynamic properties

Calculated phonon spectra provide input for assessing the thermodynamic properties. Here, we focus on the decomposition of the alkali-metal *closo*-dodecaborates into elements according to the reaction:

$$X_2B_{12}H_{12} \rightarrow 2X + 12B + 6H_2 \quad (1)$$

where X:Na, Li. The methodology of thermodynamic analysis is presented in ESI†.

The enthalpy of formation ΔH^{0K} for $Li_2B_{12}H_{12}$ is 1.173 eV/H_2, 1.248 eV/H_2, 1.255 eV/H_2 as calculated with with PBE, PBE-D2 and vdW-DF methods respectively (ΔH^{298K} is 1.235 eV/H_2, 1.256 eV/H_2, 1.316 eV/H_2 respectively). This is well compared to the analysis of Lee[58] with ΔH^{298K} =1.23 eV/H_2 with PBE method. For the decomposition reaction $Li_2B_{12}H_{12} \rightarrow 2LiH + 12B + 5H_2$, ΔH^{0K} calculated with PBE, PBE-D2 and vdW-DF methods is 1.091 eV/H_2, 1.038 eV/H_2, 1.138 eV/H_2 respectively. Previous calculations report 1.134 eV/H_2 with PW91[59] and 1.296 eV/H_2 with PBE[60]. For $Na_2B_{12}H_{12}$ the calculated enthalpy ΔH^{0K} is 1.227 eV/H_2, 1.240 eV/H_2, 1.295 eV/H_2 for PBE, PBE-D2 and vdW-DF method respectively (ΔH^{298K} is 1.292 eV/H_2, 1.306 eV/H_2, 1.361 eV/H_2, respectively). These are somehow higher than previous calculation[58] with PW91/PBE(1.138 eV/H_2).

The temperature dependence of the Gibbs free energy for the decomposition reaction (1) is shown in Fig. 5 for both compounds. The highest stability is observed for free energy calculated with vdW-DF method; all computational approaches place decomposition above experimental temperature that is 923 K[61] - 973 K[55] for $Li_2B_{12}H_{12}$. The decomposition of $Na_2B_{12}H_{12}$ takes place at even higher temperatures[55] which agrees with our results shown in Fig.5. This higher than experimentally observed decomposition temperature is related to the fact that real systems decompose to intermediate phases, like metal hydrides. Additionally, the validity of harmonic approximation at such high temperatures is limited.

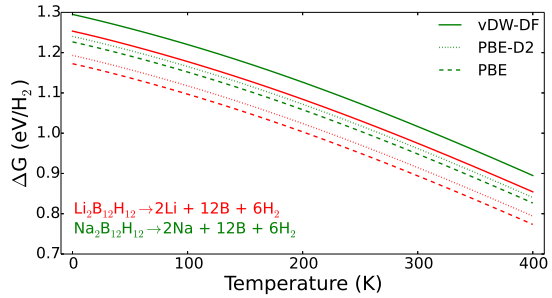

Fig. 5 The Gibbs free energy of the decomposition to elements of $Li_2B_{12}H_{12}$ (red) and $Na_2B_{12}H_{12}$(green). Solid lines are for vdW-DF method, dotted lines are for PBE-D2 and the dashed lines for PBE method. $\Delta G = 0$ at $T = 1090$ K and $T = 1160$ K with PBE for $Li_2B_{12}H_{12}$ and $Na_2B_{12}H_{12}$ respectively.

3.2 $MgB_{12}H_{12}$

The $MgB_{12}H_{12}$ is a more elusive compound than alkali metal *closo*-boranes. This compound was suggested by Li *et al.*[62] as an intermediate product of $Mg(BH_4)_2$ decomposition. Several experimental reports discuss the properties and characterization of this compound[63,64], however to the best of our knowledge there is no experimental evidence of $MgB_{12}H_{12}$ synthesis in anhydrous, pure crystalline form. The water containing samples are well characterized as $Mg(H_2O)_6B_{12}H_{12}{\cdot}6H_2O$ adapting NaTl-type ion arrangement with the symmetry $F4_132$ (Z=8)[65]. Several polymorphs without non-bonded water molecules $Mg(H_2O)_6B_{12}H_{12}$ are reported[66]. Amorphous, pure $MgB_{12}H_{12}$ was synthesized by sintering $Mg(BH_4)_2$, Mg and $B_{10}H_{14}$ in a stoichiometric molar ratio of 1 : 1 by He *et al.*[67]. The pure $MgB_{12}H_{12}$ compound was identified by resonance at -15.0 ppm in solid state ^{11}B MAS NMR spectra. However, Raman spectra showed only very broad peaks around 751 cm^{-1} and 2569 cm^{-1}. Moreover the decomposition pathway of this compound was different from $MgB_{12}H_{12}$ obtained as an intermediate product of $Mg(BH_4)_2$ decomposition. Anhydrous magnesium dodecaborane decomposes below 1073 K. Thus, it provides evidence that $MgB_{12}H_{12}$ does not form as a stable dehydrogenation product of magnesium borohydride [64,67]. This situation opens a question about the possibility of $MgB_{12}H_{12}$ synthesis in a pure anhydrous crystalline form. Such compound would be interesting as a potential magnesium ionic conductor. This question was recently addressed by Lu and Ciucci[18] who, by theoretical calculations based on hypothetical crystal structure, concluded very low magnesium mobility.

Contrary to the experiment, there exist large record of theoretical studies related to the structure of $MgB_{12}H_{12}$. Structural predictions, based on Monte Carlo configuration sampling, suggest C2/*m* crystal structure of $MgB_{12}H_{12}$[59]. The $P2_1/c$ symmetry was also suggested for $MgB_{12}H_{12}$ by a combination of experimental and DFT structure predictions[68]. These crystalline structures were questioned in *ab initio* molecular dynamics studies[69]. The authors generated 202 different crystal structures for $MgB_{12}H_{12}$ and $CaB_{12}H_{12}$ in the supercell with four formula units. For $MgB_{12}H_{12}$ a broad range of structures with specific density ranging from 750 to 1000 kg/m^3 (275 – 370 Å^3/f.u.) was predicted. All reported structures possess ground state energies varying within 0.1 eV per formula unit. However, 30% scatter of crystal densities for $MgB_{12}H_{12}$ is significantly larger than 9% for $CaB_{12}H_{12}$. Taking into account larger mass of calcium the low density of magnesium dodecaborane reported in[69] is puzzling: $CaB_{12}H_{12}/MgB_{12}H_{12}$ mass ratio is ≈1.095, while the predicted crystal densities ratio ranges from 1.35 to 1.60[69].

In order to clarify these intriguing aspects of magnesium *closo*-borane, possible crystal structures of magnesium dodeca-borane are studied with methods accounting for non-local interactions described above. We use systematic approach to the structural search by generating four groups of candidate crystal structures of $MgB_{12}H_{12}$: they are based on packing of $B_{12}H_{12}^{2-}$ anions in a simple cubic, *bcc*, *ccp*, and *hcp* configurations; additional structure is based on previously predicted C2/*m* phase. For the simple cubic system we used CsCl type ion arrangement, for *bcc* AgI initial ion arrangements, zinc blende was used for *ccp*, and wurtzite structure for *hcp* anion configuration. The initial density of all structures was set to 260 Å^3/f.u. These initial configurations were optimized with respect to internal atomic positions, during this optimization the high symmetry of parent structures was not preserved due to presence of icosahedral anion. Thus optimization changed the initial coordination number for cations as well as orientation of the anions. Subsequently the volume of each unit cell was optimized, followed by the optimization of the internal atomic positions. The procedure was repeated un-

til the convergence of 0.01 eV/Å was achieved. These optimized structures were subject to simulated annealing (heating to 300 K and cooling to 0 K). The final structures were re-optimized with the procedure as above. Finally the optimization of all degrees of freedom, including the lattice parameters was performed. The symmetry of the optimized structures were analyzed with FINDSYM software [70]. All structures were re-optimized with symmetry constraints and in the final step the symmetry was removed during optimization.

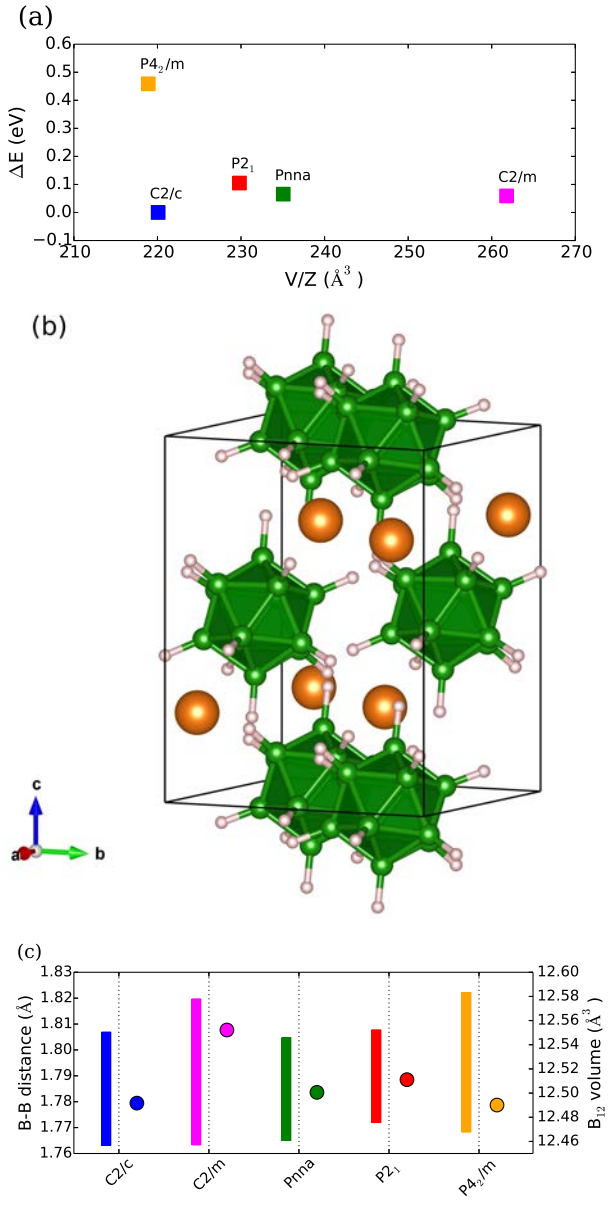

Fig. 6 The relative ground state energy and specific volume per formula unit for the most stable structures of $MgB_{12}H_{12}$ (a); The schematic view of the C2/c unit cell (b). Magnesium, boron and hydrogen atoms are denoted with orange, green and light pink color respectively. The volume of the B_{12} icosahedral cage (circles) and the range of the nearest B-B distances (vertical bars) for $MgB_{12}H_{12}$. All data calculated with the vdW-DF method, the same color coding in (a) and (c) is used.

This procedure provides the following candidate structures of $MgB_{12}H_{12}$: the $P2_1$ (Z=2) symmetry resulted from a simple cubic, CsCl initial configuration; $C2/c$ (Z=4) based on *bcc* anion configuration; P*nna* (Z=4) originated from wurtzite *hcp*, and $P4_2m$ (Z=2) that resulted from zinc blende (*ccp*). The $C2/m$ (Z=2) structure remain in the initial symmetry. The structure parameters for all phases are presented in Tables ST3 - ST7 (ESI†). The density of all new structures is higher than previously reported $C2/m$ phase, see Fig. 6. They are also 25% - 68% denser than amorphous structures reported by Kulkarni *et al.* [69]. The structures with highest density (∼1250kg/m^3) have $C2/c$ and $P4_2m$ symmetry. The structure with the lattice in $C2/c$ symmetry has the lowest ground state energy, it is also more stable than $C2/m$ by 0.06 eV. The monoclinic $C2/c$ symmetry is the same as for $CaB_{12}H_{12}$ [71] but the orientation of the cell is different. All four predicted structures differ by coordination of Mg cation: it is coordinated to two anions for $C2/m$ phase, in $P2_1$ and Pnna magnesium is located on the plane between three anions, and coordination close to tetrahedral is present in the densest $P4_2m$ and $C2/c$ structures. In fact two monoclinic structures $C2/m$ and $C2/c$ are not related by group/subgroup relations but they can be transformed to each other, for example by shrinking the c axis of $C2/m$ and bringing ionic chains closer together. These structures are visualized in Fig. S8 (ESI†). A similar analysis, as in Fig. 2, on the volume of the B_{12} cage, as well as the range of the B-B distances is shown in Fig. 6c for all the presented $MgB_{12}H_{12}$ structure. The distortion of the B_{12} cage is apparent from the wider range of the B-B distances. On the other hand, the volume of the cage ranges from 12.49^3 to 12.55^3 and compares well with the 12.48^3 and 12.51^3 of $Li_2B_{12}H_{12}$ and $Na_2B_{12}H_{12}$ respectively. Particularly for the $C2/c$ structure; the B_{12} cage volume is 12.49^3, the B-B distances range from 1.76Å to 1.81Å, the nearest distance between the centers of the $B_{12}H_{12}{}^{2-}$ anions is 6.60Å, and the nearest distance between the cations and the anions is 3.71Å. The stability of all structures was also calculated with PBE, PBE-D2, and PBE-D2* approximations to exchange - correlation functional, presented in Fig. S9 (ESI†). For PBE functional the $C2/m$ phase has the lowest ground state energy, in agreement with previous report by Ozoliņš *et al.* [59]. The PBE-D2 method underestimates the equilibrium volume per formula unit by 15% to 20% but properly reproduces the lowest ground state energy for $C2/c$ structure. This method is applied for the structures in the constrained density (PBE-D2*) the ground state energy differences are similar to these from vdW-DF method, with slightly higher energy for previously reported $C2/m$ phase.

The non-covalent interactions analysis performed for ground state structure of $MgB_{12}H_{12}$ is depicted in Fig. S6 (ESI†). The reduced density gradient plot reveals rich features around $\lambda = 0$ that indicate Van der Waals interactions. The real space visualization (Fig. S6(g,i)) (ESI†) of isosurfaces indicate stronger dispersive interactions in this compound than in $Li_2B_{12}H_{12}$. These interaction are present for anion - anion as well as for cation - anion contacts.

Phonon density of states are presented in Fig.7 for the $C2/c$ structure. The lattice modes extend to 250 cm^{-1}; internal $B_{12}H_{12}{}^{2-}$ modes span in the range from 500 cm^{-1} to 1130 cm^{-1}, similar to $LiB_{12}H_{12}$. The structure of the internal vibrations is

very similar to the one for alkali metal *closo*-borates, Fig. 4. The

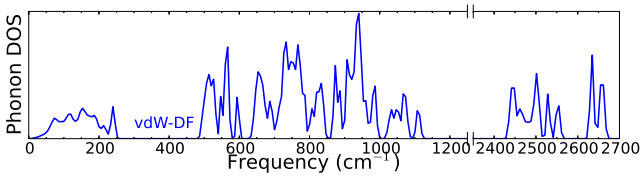

Fig. 7 The phonon density of states for $MgB_{12}H_{12}$ in C2/c symmetry.

major difference can be observed in the highest frequency region of B-H stretching vibrations. These frequencies are grouped in two regions, with the highest modes extending to 2670 cm^{-1}. This splitting originates from strong interactions between Mg cation and nearest hydrogen atoms. In fact Mg-H separation is as short as 2.02 Å (2x) and 2.15 Å (4x). Additional mode splitting is present in each of the groups. Gibbs free energy calculated from the phonon density of states indicates that the decomposition of $MgB_{12}H_{12}$ into elements or MgH_2 takes place only above 700 K, see Fig. S10 (ESI†). This analysis indicates that $Mg(BH_4)_2$ decomposes to $MgB_{12}H_{12}$ above 200 K; thus within harmonic approximation magnesium *closo*-dodecaborate is stable between 200 K and 700 K.

For complete characterization of new phases of $MgB_{12}H_{12}$ elastic properties were calculated, see Table ST8 (ESI†). In agreement with predicted crystal density the largest bulk modulus is for the densest phases: C2/c (23.91 GPa) and P4$_2$/m (25.39 GPa). The shear modulus is of the order 10.1 GPa - 14.62 GPa. The low density C2/m structure is significantly softer, see Table ST8 (ESI†).

4 Conclusions

Theoretical prediction of materials' structure and properties slowly becomes a routine task, however accuracy of used approximations shall be always carefully considered. In this work, we present a detailed accuracy assessment of DFT in description of Li, Na and Mg salts with $B_{12}H_{12}^{2-}$ anions. Accurate ground state crystal structure calculations for these compounds require cutoff energies of the plane wave basis set two or three times larger than recommended for PAW potentials. The charge density analysis directly indicates the presence of weak Van der Waals interactions between the anions of these compounds. They originate from the aromatic nature of the deltahedral molecules ($B_{12}H_{12}^{2-}$) which requires consideration of the weak dispersion forces. We show that the most accurate description of the solid state structure of these salts is provided by non-local method, and pairwise Van der Waals corrections underestimate lattice parameters. Analysis of the dynamical properties indicates a better description of atomic excitations with non-local exchange - correlation functionals. Thus, we conclude that the static and dynamical properties of these compounds can be described better with non-local exchange - correlation functionals. Semi-local methods can provide satisfactory results when applied in structure proper densities. Thus these computationally efficient methods can be used for superionic properties studies in disordered high temperature phases.

An extensive structural search for stable crystalline phases of $MgB_{12}H_{12}$ predicts new dense structure with C2/c symmetry as well as three other high density structures. They are stabilized by Van der Waals interactions. A thorough computational characterization of dynamical and elastic properties indicate stability of predicted structure with C2/c symmetry. Prediction of this and three other high density structures might allow synthesis of an anhydrous $MgB_{12}H_{12}$ in the high pressure experiments, avoiding amorphous state at ambient pressure.

5 Conflicts of interest

We have no conflicts of interest to declare.

6 Acknowledgments

SNF Sinergia project CRSII2_160749/1 and CPU allocation at PL-Grid infrastructure are kindly acknowledged.

References

1 J. W. Johnson and M. S. Whittingham, *J. Electrochem. Soc.*, 1980, **127**, 1653–1654.
2 T. J. Udovic, M. Matsuo, A. Unemoto, N. Verdal, V. Stavila, A. V. Skripov, J. J. Rush, H. Takamura and S.-i. Orimo, *Chem. Commun.*, 2014, **50**, 3750–3752.
3 J. Janek and W. G. Zeier, *Nat. Energy*, 2016, **1**, 16141.
4 K. Yoshida, T. Sato, A. Unemoto, M. Matsuo, T. Ikeshoji, T. J. Udovic and S.-i. Orimo, *Appl. Phys. Lett.*, 2017, **110**, 103901.
5 L. Duchêne, R.-S. Kühnel, D. Rentsch, A. Remhof, H. Hagemann and C. Battaglia, *Chem. Commun.*, 2017, **53**, 4195–4198.
6 W. S. Tang, K. Yoshida, A. V. Soloninin, R. V. Skoryunov, O. A. Babanova, A. V. Skripov, M. Dimitrievska, V. Stavila, S.-i. Orimo and T. J. Udovic, *ACS Energy Lett.*, 2016, **1**, 659–664.
7 W. S. Tang, A. Unemoto, W. Zhou, V. Stavila, M. Matsuo, H. Wu, S.-i. Orimo and T. J. Udovic, *Energy Environ. Sci.*, 2015, **8**, 3637–3645.
8 M. Brighi, F. Murgia, Z. Łodziana, P. Schouwink, A. Wolczyk and R. Černý, *submitted*.
9 V. Thangadurai, S. Narayanan and D. Pinzaru, *Chem. Soc. Rev.*, 2014, **43**, 4714–4727.
10 N. Kamaya, K. Homma, Y. Yamakawa, M. Hirayama, R. Kanno, M. Yonemura, T. Kamiyama, Y. Kato, S. Hama, K. Kawamoto and A. Mitsui, *Nat. Mat.*, 2001, **10**, 682.
11 N. Verdal, J.-H. Her, V. Stavila, A. V. Soloninin, O. A. Babanova, A. V. Skripov, T. J. Udovic and J. J. Rush, *J. Solid State Chem.*, 2014, **212**, 81 – 91.
12 W. Lipscomb, *Boron Hydrides*, Benjamin, New York, 1963.
13 K. Wade, *Advances in Inorganic Chemistry and Radiochemistry*, Academic Press, 1976, vol. 18, pp. 1 – 66.
14 J. Aihara, *J. Am. Chem. Soc.*, 1978, **100**, 3339–3342.
15 R. B. King, *Chem. Rev.*, 2001, **101**, 1119–1152.
16 J. B. Varley, K. Kweon, P. Mehta, P. Shea, T. W. Heo, T. J. Udovic, V. Stavila and B. C. Wood, *ACS Energy Lett.*, 2017, **2**, 250–255.
17 Z. Lu and F. Ciucci, *J. Mater. Chem. A*, 2016, **4**, 17740–17748.

18 Z. Lu and F. Ciucci, *Chem. Mat.*, 2017, **29**, 9308–9319.

19 K. E. Kweon, J. B. Varley, P. Shea, N. Adelstein, P. Mehta, T. W. Heo, T. J. Udovic, V. Stavila and B. C. Wood, *Chem. Mat.*, 2017, **29**, 9142–9153.

20 Y. Sadikin, P. Schouwink, M. Brighi, Z. Łodziana and R. Cerný, *Inorg. Chem.*, 2017, **56**, 5006–5016.

21 S. Grimme, J. Antony, S. Ehrlich and H. Krieg, *J. Chem. Phys.*, 2010, **132**, 154104.

22 S. Grimme, S. Ehrlich and L. Goerigk, *J. Comput. Chem.*, 2011, **32**, 1456–1465.

23 M. Dion, H. Rydberg, E. Schröder, D. C. Langreth and B. I. Lundqvist, *Phys. Rev. Lett.*, 2004, **92**, 246401.

24 A. M. Reilly and A. Tkatchenko, *Chem. Sci.*, 2015, **6**, 3289–3301.

25 J. Tao, Y. Mo, G. Tian and A. Ruzsinszky, *Phys. Rev. B*, 2016, **94**, 085126.

26 W. I. F. David, R. M. Ibberson, J. C. Matthewman, K. Prassides, T. J. S. Dennis, H. W. Hare, Jonathan P.and Kroto, R. Taylor and D. R. M. Walton, *Nature*, 1991, **353**, 147 – 149.

27 G. Kresse and J. Hafner, *Phys. Rev. B*, 1993, **47**, 558–561.

28 G. Kresse and J. Hafner, *Phys. Rev. B*, 1994, **49**, 14251–14269.

29 G. Kresse and J. Furthmüller, *Comput. Mater. Sci.*, 1996, **6**, 15 – 50.

30 G. Kresse and J. Furthmüller, *Phys. Rev. B*, 1996, **54**, 11169–11186.

31 G. Román-Pérez and J. M. Soler, *Phys. Rev. Lett.*, 2009, **103**, 096102.

32 J. Klimeš, D. R. Bowler and A. Michaelides, *Phys. Rev. B*, 2011, **83**, 195131.

33 K. Berland, V. R. Cooper, K. Lee, E. Schröder, T. Thonhauser, P. Hyldgaard and B. I. Lundqvist, *Rep. Prog. Phys.*, 2015, **78**, 066501.

34 C. Adamo and V. Barone, *J. Chem. Phys.*, 1999, **110**, 6158–6170.

35 A. V. Krukau, O. A. Vydrov, A. F. Izmaylov and G. E. Scuseria, *J. Chem. Phys.*, 2006, **125**, 224106.

36 H. C. Longuet-Higgins and J. Roberts, *Proc. Royal Soc. A*, 1955, **230**, 110–119.

37 J. A. Wunderlich and W. N. Lipscomb, *J. Am. Chem. Soc.*, 1960, **82**, 4427–4428.

38 E. L. Muetterties, R. E. Merrifield, H. C. Miller, W. H. Knoth and J. R. Downing, *J. Am. Chem. Soc.*, 1962, **84**, 2506–2508.

39 W. N. Lipscomb, *Science*, 1977, **196**, 1047–1055.

40 B. R. Hansen, M. Paskevicius, H.-W. Li, E. Akiba and T. R. Jensen, *Coord. Chem. Rev.*, 2016, **323**, 60 – 70.

41 S.-J. Hwang, R. C. Bowman, J. W. Reiter, Rijssenbeek, G. L. Soloveichik, J.-C. Zhao, H. Kabbour and C. C. Ahn, *J. Phys. Chem. C*, 2008, **112**, 3164–3169.

42 J.-H. Her, M. Yousufuddin, W. Zhou, S. S. Jalisatgi, J. G. Kulleck, J. A. Zan, S.-J. Hwang, R. C. Bowman and T. J. Udovic, *Inorg. Chem.*, 2008, **47**, 9757–9759.

43 M. Paskevicius, M. P. Pitt, D. H. Brown, D. A. Sheppard, S. Chumphongphan and C. E. Buckley, *Phys. Chem. Chem. Phys.*, 2013, **15**, 15825–15828.

44 J.-H. Her, W. Zhou, V. Stavila, C. M. Brown and T. J. Udovic, *J. Phys. Chem. C*, 2009, **113**, 11187–11189.

45 A. Bil, B. Kolb, R. Atkinson, D. G. Pettifor, T. Thonhauser and A. N. Kolmogorov, *Phys. Rev. B*, 2011, **83**, 224103.

46 Z. Łodziana and M. J. van Setten, *Phys. Rev. B*, 2010, **81**, 024117.

47 H. Hamaker, *Physica*, 1937, **4**, 1058 – 1072.

48 J. P. Perdew and A. Zunger, *Phys. Rev. B*, 1981, **23**, 5048–5079.

49 J. P. Perdew, K. Burke and M. Ernzerhof, *Phys. Rev. Lett.*, 1996, **77**, 3865–3868.

50 I. Tiritiris, T. Schleid, K. Müller and W. Preetz, *Z. Anorg. Allg. Chem*, 2000, **626**, 323–325.

51 I. Tiritiris and T. Schleid, *Z. Anorg. Allg. Chem*, 2003, **629**, 1390–1402.

52 A. D. Becke and K. E. Edgecombe, *J. Chem. Phys.*, 1990, **92**, 5397–5403.

53 E. R. Johnson, S. Keinan, P. Mori-Sànchez, J. Contreras-García, A. J. Cohen and W. Yang, *J. Am. Chem. Soc.*, 2010, **132**, 6498–6506.

54 L. He, H.-W. Li, H. Nakajima, N. Tumanov, Y. Filinchuk, S.-J. Hwang, M. Sharma, H. Hagemann and E. Akiba, *Chem. Mater.*, 2015, **27**, 5483–5486.

55 L. He, H.-W. Li and E. Akiba, *Energies*, 2015, **8**, 12429–12438.

56 M. Sharma, D. Sethio, V. D'Anna and H. Hagemann, *Int. J. Hydrogen Energy*, 2015, **40**, 12721 – 12726.

57 J. P. Merrick, D. Moran and L. Radom, *J. Phys. Chem. A*, 2007, **111**, 11683–11700.

58 T. B. Lee, *Computational Investigation of Condensed Phase Properties of Ionic Systems*, PhD Thesis, Aubur University, 2012.

59 V. Ozoliņš, E. H. Majzoub and C. Wolverton, *J. Am. Chem. Soc.*, 2009, **131**, 230–237.

60 N. Ohba, K. Miwa, M. Aoki, T. Noritake, S.-i. Towata, Y. Nakamori, S.-i. Orimo and A. Züttel, *Phys. Rev. B*, 2006, **74**, 075110.

61 M. P. Pitt, M. Paskevicius, D. H. Brown, D. A. Sheppard and C. E. Buckley, *J. Am. Chem. Soc.*, 2013, **135**, 6930–6941.

62 H.-W. Li, K. Kikuchi, Y. Nakamori, N. Ohba, K. Miwa, S. Towata and S. Orimo, *Acta Mater.*, 2008, **56**, 1342 – 1347.

63 A. Remhof, Y. Yan, D. Rentsch, A. Borgschulte, C. M. Jensen and A. Zuttel, *J. Mater. Chem. A*, 2014, **2**, 7244–7249.

64 Y. Yan, A. Remhof, D. Rentsch and A. Züttel, *Chem. Commun.*, 2015, **51**, 700–702.

65 I. Tiritiris and T. Schleid, *Z. Anorg. Allg. Chemie*, 2004, **630**, 541–546.

66 E. Didelot, Y. Sadikin, Z. Łodziana and R. Černý, *submitted*.

67 L. He, H.-W. Li, N. Tumanov, Y. Filinchuk and E. Akiba, *Dalton Trans.*, 2015, **44**, 15882–15887.

68 H.-W. Li, K. Miwa, N. Ohba, T. Fujita, T. Sato, Y. Yan, S. Towata, M. W. Chen and S. Orimo, *Nanotechnology*, 2009, **20**, 204013.

69 A. D. Kulkarni, L.-L. Wang, D. D. Johnson, D. S. Sholl and J. K. Johnson, *J. Phys. Chem. C*, 2010, **114**, 14601–14605.

70 H. T. Stokes and D. M. Hatch, *J. Appl. Crystallography*, 2005, **38**, 237–238.
71 V. Stavila, J.-H. Her, W. Zhou, S.-J. Hwang, C. Kim, L. A. M. Ottley and T. J. Udovic, *J. Solid State Chem.*, 2010, **183**, 1133 – 1140.